Differential conductance through a NINS junction on graphene

2008 J. Phys.: Condens. Matter 20 445220

(http://iopscience.iop.org/0953-8984/20/44/445220)

IOP PUBLISHING JOURNAL OF PHYSICS: CONDENSED MATTER

J. Phys.: Condens. Matter **20** (2008) 445220 (5pp) doi:10.1088/0953-8984/20/44/445220

Differential conductance through a NINS junction on graphene

Zhi-Yong Zhang

Department of Physics, Nanjing University, Nanjing 210093, People's Republic of China

Received 7 July 2008, in final form 12 September 2008
Published 10 October 2008
Online at stacks.iop.org/JPhysCM/20/445220

Abstract

The differential conductance through a normal metal–insulator–normal metal–superconductor (NINS) junction on graphene is obtained via numerical calculation of the Dirac–Bogoliubov–de Gennes equation. A series of sub-gap peaks of differential conductance can be found no matter whether the Andreev reflection is specular or standard. In the meantime, the differential conductance displays an oscillatory behaviour as a function of the effective barrier strength even if the Fermi surface mismatch is large. In the two limiting situations with the superconducting gap much smaller or much larger than the Fermi energy, all of the oscillations are in the same phase, and the number and positions of the sub-gap peaks are determined only by the distance between the NI and NS interfaces. In the intermediate regime with the Andreev retro-reflection crossing over to a specular one, however, a phase shift appears between any two different oscillations. The number and positions of the sub-gap peaks are related not only to that distance but also to the effective barrier strength.

(Some figures in this article are in colour only in the electronic version)

1. Introduction

Recent fabrication of graphene [1], a monatomic layer of graphite with a honeycomb lattice structure, provides the opportunity to employ its unusual low-energy electronic properties to the design of novel micro-electronic devices. Undoped graphene has six discrete Fermi points, corresponding to the corners of the hexagonal Brillouin zone, out of which only two are inequivalent. In the vicinity of these two valleys, the excitation spectrum obeys a Dirac-like Hamiltonian [2, 3], which yields a linear energy dispersion instead of a parabolic one. The electronic and hole states are interconnected, and chirality, the projection of pseudo-spin on the direction of motion, is conserved in the tunnelling process [4]. These unusual low-energy electronic properties lead to the novel transport behaviour in micro-electronic devices based on graphene.

State-of-the-art fabrication technology can induce superconductivity in graphene via the proximity effect [5, 6]. It is of theoretical interest and of technological importance to investigate how the unusual low-energy electronic properties affect charge transport under the influence of superconductivity. Beenakker [7] found that in a normal metal–superconductor (NS) junction on graphene, the Andreev reflection is not always retro-reflection [8] but can be specular if the superconducting gap Δ is much larger than the Fermi energy E_F of the N region [9]. Bhattacharjee and Sengupta [10] found that the conductance through a NIS junction on graphene, where I, an 'insulator' layer, is modelled as a thin barrier, displays an oscillatory behaviour as a function of the effective barrier strength, although this I layer acts as a counterpart of the δ potential for non-relativistic particles. The difference comes from the quantum interference effect, which is permitted in the 'insulator' layer due to the linear dispersion but prohibited in the δ potential. The amplitude of these oscillations is maximum for aligned Fermi surfaces of the N and S regions and vanishes for a large Fermi surface mismatch. Linder and Sudbø [11] also calculated the differential conductance through a NIS junction on graphene, but in their model the 'insulator' layer is wide and the S region may have unconventional pairing potential. A series of sub-gap differential conductance peaks can be found for both s- and d-wave pairing because of the quantum interference taking place in the 'insulator' layer.

Another typical structure in the study of the transport properties of non-relativistic particles is a NINS junction with I modelled as a δ function. The Andreev retro-reflection at the NS interface and the normal specular reflection at the δ function can construct a round-trip path, which results in a series of sub-gap differential conductance peaks due to the formation of Andreev bound states [12]. For a NINS junction on graphene with I a thin 'insulator' layer, the round-trip path

cannot be formed if Andreev reflection is specular. In a naive viewpoint, the sub-gap differential conductance peaks can only be found with $\Delta \ll E_F$. But even with specular Andreev reflection, multiple scatterings still take place between the NS and NI interfaces. Whether sub-gap differential conductance peaks can be found, and if they can what their characteristics are in the situations with $\Delta \ll E_F$ and $\Delta \gg E_F$ and in the intermediate regime with the Andreev retro-reflection crossing over to a specular one, are two questions that need to be clarified. Multiple scatterings can also take place in the I layer for relativistic particles. With the I layer moving away from the NS interface, the multiple scatterings in the two regions interplay with each other. How the quantum interference effect in the whole structure influences the oscillatory behaviour of differential conductance in the three different regimes is another question needing to be clarified.

The purpose of the present work is to answer these questions. Via numerical calculation of the Dirac–Bogoliubov–de Gennes (DBdG) equation [7, 10, 11] we find that, as expected, a series of sub-gap peaks of differential conductance can be formed no matter whether the Andreev reflection is specular or standard. In the meantime, the differential conductance displays an oscillatory behaviour as a function of the effective barrier strength even if the Fermi surface mismatch is large. In the two limiting situations with $\Delta \ll E_F$ and $\Delta \gg E_F$, all of these oscillations are in the same phase and the number and positions of sub-gap peaks are determined only by the distance between the NI and NS interfaces. In the intermediate regime, however, although all of the oscillations still have a common period a phase shift can be found between any two different oscillations. The number and positions of the sub-gap peaks are related not only to that distance but also to the effective barrier strength.

The organization of this paper is as follows. In section 2, the theoretical model is presented. In section 3, the numerical results are illustrated and discussed. A brief summary is given in section 4.

2. Model and formulae

In the present paper we calculate the differential conductance through a NINS junction formed on a graphene sheet, which is assumed as the xy plane. The left half sheet $x < 0$ is in the normal (N), whereas the right half sheet $x > 0$ is covered by a superconducting electrode (S), which induces superconductivity in the graphene sheet by means of the proximity effect [5, 6]. Neglecting the self-consistency of spatial distribution of the pair potential in the S layer [7, 10, 11], we take the pair potential as $\Delta(\vec{r}) = \Delta\Theta(x)$ with $\Theta(x)$ the Heaviside step function. The electrostatic potentials in the left and right half sheets can be adjusted independently by gate voltages or by doping, so that the potential of the left half sheet has a difference U from that of the right half one. The Fermi length in the former is $\lambda_F = 2\pi\hbar v_F/E_F$, whereas it is $\lambda'_F = 2\pi\hbar v_F/(E_F + U)$ in the latter with E_F the Fermi energy. A thin 'insulator' layer (I), modelled as a square potential barrier, extends from $x = -(L + d)$ to $x = -L$. This I layer separates the left half sheet into three parts: the left N, I and central N regions. The effective barrier strength is defined as $\chi = V_B d/(\hbar v_F)$ with V_B the barrier height, which can be adjusted by another gate voltage or by additional doping. Here, the barrier width d is much smaller than λ_F.

In the absence of impurity scattering, such a NINS junction on graphene can be described by the DBdG equation as [7, 13]

$$\begin{pmatrix} \hat{H}_\pm - E_F + V(\vec{r}) & \Delta(\vec{r}) \\ \Delta^*(\vec{r}) & E_F - V(\vec{r}) - \hat{H}_\pm \end{pmatrix} \Psi_\pm = E\Psi_\pm \quad (1)$$

with $\hat{H}_\pm = -i\hbar v_F(\hat{\sigma}_x\partial_x \pm \hat{\sigma}_y\partial_y)$. Here $\pm$ refers to the two inequivalent valleys K and K', and $v_F \approx 10^6$ m s^{-1}. The Pauli matrices operate in the pseudo-spin space, corresponding to the A and B atoms of honeycomb structures. $V(\vec{r}) = V_B\Theta(x + d + L)\Theta(-x - L) - U\Theta(x)$. The excitation energy E is measured from the Fermi energy E_F. The mean-field description of superconductivity implicitly imposes a restriction $\Delta \ll E_F + U$. It is satisfied when $\Delta \ll E_F$ even if $U = 0$, but it is also satisfied when $\Delta \gg E_F$ only if $\Delta \ll U$. In the later situation, the specular Andreev reflection takes place at the NS interface. In writing the above equation, the spin index is omitted due to the spin degeneracy. Because of the valley degeneracy [7, 14], it is sufficient to consider either one of the two sets in the equation (1). Hereafter for clarity, only $\hat{H}_+$ is considered and the subscript $+$ is omitted.

When an electron with energy E is incident from the left N region with an angle θ^e, the total wavefunction is a superposition of electronic and hole excitations due to the Andreev reflection. In the left and central N regions, the states of electronic and hole excitations are: $\phi^e(\theta^e) = \frac{1}{\sqrt{2}}(1, e^{i\theta^e}, 0, 0)^T e^{ik^e\cos\theta^e x}$ and $\phi^h(\theta^h) = \frac{1}{\sqrt{2}}(0, 0, 1, -e^{i\theta^h})^T e^{ik^h\cos\theta^h x}$, where $k^\nu = (E \pm E_F)/(\hbar v_F)$ and $\theta^\nu = \sin^{-1}(k_y/k^\nu)$ with the signs $+$ and $-$ corresponding to $\nu = e$ and h, respectively. Here, $k_y = k^e \sin\theta^e$, the wavevector in the transverse direction, is conserved in the tunnelling process. Due to the mirror symmetry with respect to the xz plane, θ^e can be restricted in $[0, \pi/2]$. In the above states, a common factor $e^{ik_y y}$ is omitted for clarity. If $\theta^e > \theta^e_c = \sin^{-1}|k^h/k^e|$ for $|k^h| < |k^e|$, the Andreev reflection is forbidden. The total wavefunction in the left N region can be written as

$$\Psi = \phi^e(\theta^e) + r\phi^e(\tilde{\theta}^e) + r^A\phi^h(\tilde{\theta}^h), \quad (2)$$

and it is

$$\Psi = a^e\phi^e(\theta^e) + a^h\phi^h(\theta^h) + b^e\phi^e(\tilde{\theta}^e) + b^h\phi^h(\tilde{\theta}^h) \quad (3)$$

in the central N region. Here, $\tilde{\theta}^\nu = (\pi - |\theta^\nu|)\theta^\nu/|\theta^\nu|$.

In the I layer, the states of electronic and hole excitations φ^ν have the same forms as ϕ^ν. The only difference is that k^ν and θ^ν are replaced by $p^\nu = (E \pm (E_F - V))/(\hbar v_F)$ and $\eta^\nu = \sin^{-1}(k_y/p^\nu)$, respectively. In this layer, the total wavefunction is

$$\Psi = c^e\varphi^e(\eta^e) + c^h\varphi^h(\eta^h) + d^e\varphi^e(\tilde{\eta}^e) + d^h\varphi^h(\tilde{\eta}^h) \quad (4)$$

with $\tilde{\eta}^\nu = (\pi - |\eta^\nu|)\eta^\nu/|\eta^\nu|$.

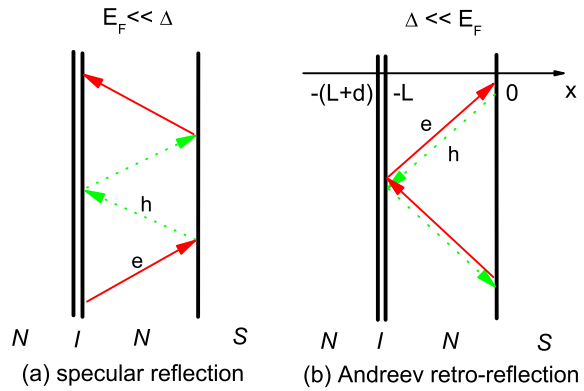

Figure 1. Schematic illustration of the reflection process in a NINS junction when specular reflection (a) and retro-reflection (b) take place at the NS interface. Here, red solid arrows correspond to the movement of an electron and green dotted ones to a hole.

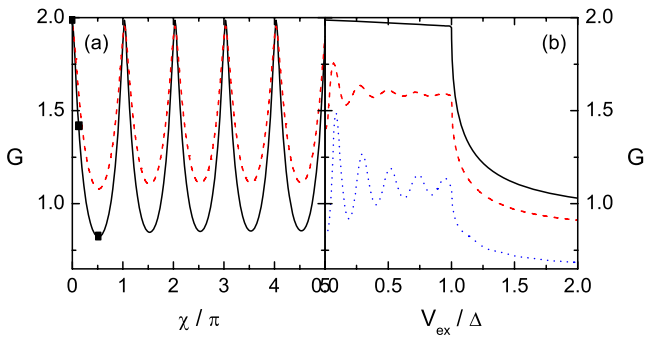

Figure 2. (a) G–χ curves for $V_{ex} = 0$ (black solid) and Δ (red dashed). (b) G–V_{ex} curves at $\chi = 0$ (black solid), 0.13π (red dashed) and 0.52π (blue dotted). These three χs are marked in (a) as filled squares. The other parameters are $E_F/\Delta = 100$, $U = 0$, $\Delta d/\hbar v_F = 0.001$ and $\Delta L/\hbar v_F = 2\pi$.

In the S region, the electron- and hole-like excitations are given as $\psi^e = (u, ue^{i\zeta^e}, v, ve^{i\zeta^e})^T e^{iq^e \cos\zeta^e x}$ and $\psi^h = (v, ve^{i\zeta^h}, u, ue^{i\zeta^h})^T e^{iq^h \cos\zeta^h x}$, respectively, where $q^\nu = (E_F \pm \sqrt{E^2 - \Delta^2})/(\hbar v_F)$ with $\zeta^\nu = \sin^{-1}[k_y/q^\nu]$. The superconductor coherent factors u and v are $u = \sqrt{[1 + E^{-1}(E^2 - \Delta^2)^{1/2}]/2}$ and $v = \sqrt{[1 - E^{-1}(E^2 - \Delta^2)^{1/2}]/2}$. Then in the S lead, the total wavefunction is

$$\Psi = t^e \psi_s^e(\zeta^e) + t^h \psi_s^h(\pi - \zeta^h). \quad (5)$$

From the boundary condition, that is the continuity of wavefunction Ψ at the interfaces, all of the superposition coefficients in the above four equations can be obtained analytically. But this process is so tedious that we prefer to do a numerical calculation. Because of the conservation of pseudo-spin projected on the propagating direction, backscattering is forbidden when an electron is normally incident into the I layer [4]. This perfect transparency is a manifestation of the Klein paradox [15] in condensed matter physics. But in experiments, the angle-resolved transmissivity cannot be measured easily, and what we are interested in is the differential conductance. Under an external bias V_{ex}, the normalized zero-temperature differential conductance can be written as [7, 10, 11, 16]:

$$G(V_{ex}) = \int_0^{\theta_c^e} d\theta^e \cos\theta^e \left(1 - |r|^2 + |r_A|^2 \frac{\cos\theta^h}{\cos\theta^e}\right), \quad (6)$$

where r and r_A are both obtained at V_{ex}.

3. Results and discussion

We first consider the situation with $\Delta \ll E_F$, then that with $\Delta \gg E_F$. In the former Andreev retro-reflection takes place, and in the latter the Andreev reflection is specular. The intermediate regime with $\Delta \approx E_F$ is also considered, where Andreev retro-reflection crosses over to a specular reflection. In our numeric calculation, the superconducting gap Δ is set as the energy unit, $\Delta d/(\hbar v_F) = 0.001$ and $\Delta L/\hbar v_F = 2\pi$.

Figure 2 presents the results for $\Delta \ll E_F$, which are obtained with $U = 0$ and $E_F/\Delta = 100$. Here, figure 2(a) gives the G–χ curves for $V_{ex} = 0$ (black solid) and $V_{ex} = \Delta$ (red dashed), and figure 2(b) plots the variations of G with the external bias V_{ex} for $\chi = 0$ (black solid), 0.13π (red dashed) and 0.52π (blue dotted). These χs are marked on the $G(0)$–χ curve as filled squares. As we can see from figure 2(a), $G(0)$ and $G(\Delta)$ oscillate in the same phase with a period π, and their maximum values appear approximately at $n\pi$. This is in contrast to a NIS junction where the amplitude of these oscillations vanishes at the gap edge with $G(\Delta) \approx 2$, The small deviation from exact $n\pi$ comes from the fact that the barrier width d taken in our numerical calculation is finite. The positions of those maximum points are independent of L, the distance between the I layer and the NS interface. Even with L decreased to zero, the maximum values are still located at $n\pi$. Although this result is different from that of [10] it is consistent with that of [11] and is reasonable from the physics, since at $\chi = 0$ the influence of the 'insulator' layer disappears. For $G(0)$ its maximum value reaches 2, and for $G(\Delta)$ it is a little smaller than 2. These results are different from the tunnelling of non-relativistic particles, where the differential conductance is suppressed with the corresponding δ potential increased and no oscillation can be found. In a NINS junction on graphene, the oscillation of differential conductance comes mainly from quantum interference in the I layer, but the contrast with a NIS junction demonstrates the interplay of multiple scatterings in the I layer and in the region between the NI and NS interfaces.

Although this multiple scattering effect cannot change the period of those oscillations, it can affect the G–V_{ex} curves. As schematically illustrated in figure 1, in the situation with $\Delta \ll E_F$, Andreev bound states are formed in a NINS junction [12]. As a result, the G–V_{ex} curves exhibit a series of sub-gap peaks for any χ except $\chi = n\pi$, where the sub-gap differential conductance is close to 2 and no peak can be found. Although the peak values oscillate with χ, the number and positions of these sub-gap peaks are independent with χ. They are only related to L. That is, these characteristics are only determined by the multiple scatterings between the NI and NS interfaces. With the Andreev retro-reflection taking place, the interference effects in the two different regions can

be considered separately, and the differential conductance of the whole structure is simply a multiplication of two factors.

Now we turn our attention to the situation with $\Delta \gg E_F$, where the Andreev reflection is specular. These results are presented in figures 3(a) and (b). Here, $U/\Delta = 100$, so that Δ is still much smaller than $E_F + U$. In this situation, the differential conductance still oscillates with χ except at $V_{ex} = 0$, where $G(0)$ is fixed as 2 (not presented in figure 3(a)). This is entirely different from the results of a NIS junction where the amplitude of those oscillations vanishes due to the large Fermi surface mismatch [10]. In a NIS junction, a large Fermi surface mismatch acts as an effective barrier which makes the presence of an additional barrier irrelevant. As a result, the amplitude of oscillations of differential conductance vanishes. Whereas in a NINS junction, although the resulted effective barrier changes the multiple scattering effect between the NI and NS interfaces, quantum interference in the I layer still plays an important role in charge transport. However, in the situation with $\Delta \gg E_F$, the period of these oscillations is still π, and at $n\pi$ they reach to their maximum values simultaneously. The multiple scatterings between the NI and NS interfaces cannot introduce phase shift between different oscillations. On the other hand, under specular Andreev reflection, although propagating modes and not Andreev bound states are formed in a NINS junction [17], the multiple scatterings between the NI and NS interfaces still lead to a series of sub-gap differential conductance peaks which can be seen clearly from the G–V_{ex} curves illustrated in figure 3(b). The basic characteristics of these peaks, such as the peak number and peak positions, are only determined by L. All of these results look like those obtained in the limit with $\Delta \ll E_F$: the differential conductance is simply a multiplication of two factors.

Figures 3(c)–(f) illustrate the results for $\Delta \approx E_F$, which are also obtained with $U/\Delta = 100$. The χs taken to obtain the corresponding G–V_{ex} curves in figures 3(b), (d) and (f) are given in table 1, and are marked as filled squares in figures 3(a), (c) and (e), respectively, where the variations of $G(0)$ and $G(\Delta)$ with χ are plotted. In the regime with the Andreev retro-reflection crossing over to a specular one, the differential conductance exhibits entirely different properties from the other two situations. As a representative, the results for $E_F/\Delta = 0.1$ are illustrated in figures 3(c) and (d). In contrast to a NIS junction where the oscillation amplitude vanishes under a large Fermi surface mismatch, both the $G(0)$–χ and $G(\Delta)$–χ curves oscillate with a period π because of the interplay of multiple scatterings in the I layer and in the region between the NI and NS interfaces. This result is similar to the situation with $\Delta \gg E_F$, but now the two oscillations are not in the same phase. For the $G(0)$–χ curve, the maximum conductance can reach a value close to 1.9, but these maximum points are not located at $n\pi$, where $G(0) = 4/3$. Only at the specific positions deviating from $n\pi$ can $G(0)$ reach its maximum value, although at these points the transmission through an isolated I layer does not reach resonance. Compared with the $G(0)$–χ curve, a phase shift appears in the $G(\Delta)$–χ curve, and asymmetry can be found in this curve. These results show that in the intermediate regime the interplay of multiple scatterings in the I layer and in the region between the NI and NS interfaces has a more complex effect on the differential conductance. Furthermore, in the G–V_{ex} curves, a series of sub-gap peaks can be found if $\chi \neq n\pi$. (Of course, at $V_{ex} = E_F$, G is zero since $\theta_c^e = 0$.) But now the peak number and peak positions are related not only to L but also to χ. In the intermediate regime, the interference effects in the two different regions cannot be considered separately, and the differential conductance of the whole structure is no longer a simple multiplication of two factors.

To further clarify the role of Fermi surface mismatch on charge transport of a NINS junction, the results for $\Delta = E_F = U/100$ are presented in figures 3(e) and (f). For any χ, $G(\Delta) = 0$ (not presented in figure 3(e)), since at $V_{ex} = \Delta$, $\theta_c^e = 0$. As in the junction with $E_F/\Delta = 0.1$ and $U/\Delta = 100$, the positions of maximum points of the $G(0)$–χ curve still deviate from $n\pi$, but now this deviation is small. In the meantime, the phase shift between different G–χ curves also

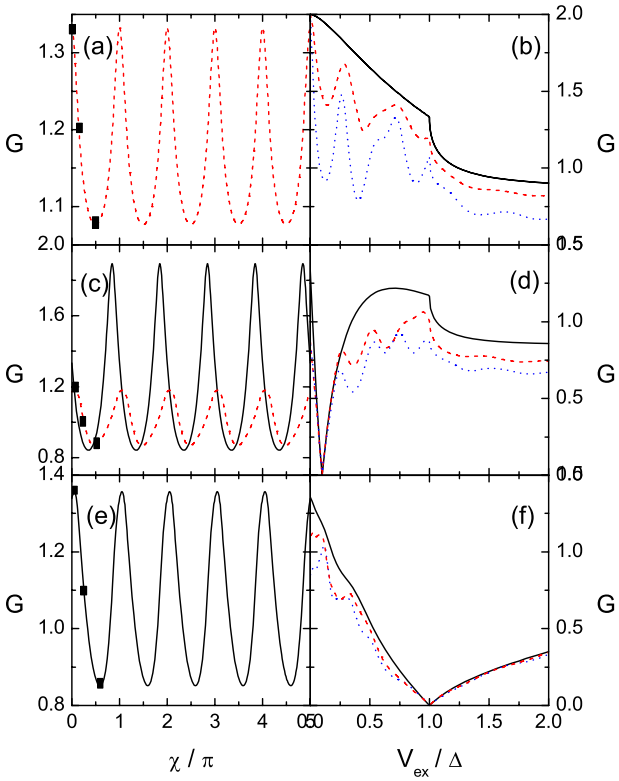

Figure 3. In the left column: $G(0)$–χ (black solid) and $G(\Delta)$–χ (red dashed) curves. In the right column: G–V_{ex} curves at different χs, which, marked as filled squares in the left column, are given in table 1. $E_F/\Delta \ll 1$ ((a) and (b)), $E_F/\Delta = 0.1$ ((c) and (d)) and $E_F/\Delta = 1$ ((e) and (f)) with the other parameters the same as in figure 2.

Table 1. The χ values adopted to obtain the G–V_{ex} curves in figures 3(b), (d) and (f). Here, χ_1 corresponds to the black solid curves, χ_2 to red dashed and χ_3 to blue dotted.

E_F/Δ	χ_1	χ_2	χ_3
$\ll 1$	0	0.15π	0.5π
0.1	0	0.25π	0.47π
1	0.05π	0.25π	0.59π

becomes small. With E_F further increased, the phase shift diminishes, so that at $\Delta \ll E_F$ all of the G–χ curves oscillate in the same phase and the maximum values appear at $n\pi$. But when $U \neq 0$, the maximum value of the $G(0)$–χ curve cannot reach 2 because of the Fermi surface mismatch across the NS interface. For example, at $E_F = U = 100\Delta$, this maximum value can reach only about 1.62. The Fermi surface mismatch only acts as an effective barrier at the NS interface, but the interplay of multiple scatterings in the two different regions still plays an important role. The phase shift between different G–χ curves and the deviation of maximum points from $n\pi$ are characteristics of the intermediate regime.

4. Summary

In summary, the differential conductance through a NINS junction on graphene is obtained via numerical calculation of the DBdG equation [7, 10, 11]. A series of sub-gap peaks of differential conductance can be found no matter whether the Andreev reflection is specular or standard. In the meantime, G oscillates with χ even if the Fermi surface mismatch between the N and S regions is large. In the two limiting situations with $\Delta \ll E_F$ and $\Delta \gg E_F$, all of the oscillations are in the same phase, and the number and positions of those sub-gap peaks are only determined by L. In the intermediate regime, however, where the Andreev retro-reflection crosses over to a specular one, a phase shift appears between any two different oscillations. The number and positions of those sub-gap peaks are related not only to L but also to χ.

Acknowledgment

This work is supported by the Natural Science Foundation of China.

References

[1] Novoselov K S *et al* 2004 *Science* **306** 666
[2] Wallace P R 1947 *Phys. Rev.* **71** 622
[3] DiVincenzo D P and Mele E J 1984 *Phys. Rev.* B **29** 1685
[4] Katsnelson M I, Novoselov K S and Geim A K 2006 *Nat. Phys.* **2** 620
[5] Heersche H B *et al* 2007 *Nature* **446** 56
[6] Du X, Skachko I and Andrei E Y 2008 *Phys. Rev.* B **77** 184507
[7] Beenakker C W J 2006 *Phys. Rev. Lett.* **97** 067007
[8] Andreev A F 1964 *Zh. Eksp. Teor. Fiz.* **46** 1823
Andreev A F 1964 *Sov. Phys.–JETP* **19** 1228 (Engl. Transl.)
[9] Cayssol J 2008 *Phys. Rev. Lett.* **100** 147001
[10] Bhattacharjee S and Sengupta K 2006 *Phys. Rev. Lett.* **97** 217001
[11] Linder J and Sudbø A 2007 *Phys. Rev. Lett.* **99** 147001
Linder J and Sudbø A 2008 *Phys. Rev.* B **77** 064507
[12] Xu J H, Miller J H Jr and Ting C S 1996 *Phys. Rev.* B **53** 3604
[13] De Gennes P G 1966 *Superconductivity of Metals and Alloys* (New York: Benjamin)
[14] Suzuura H and Ando T 2002 *Phys. Rev. Lett.* **89** 266603
[15] Klein O 1929 *Z. Phys.* **53** 157
[16] Blonder G E, Tinkham M and Klapwijk T M 1982 *Phys. Rev.* B **25** 4515
[17] Titov M, Ossipov A and Beenakker C W J 2007 *Phys. Rev.* B **75** 045417